Comparative study of domoic acid accumulation, isomer content and associated digestive subcellular processes in five marine invertebrate species

José Luis García-Corona, Hélène Hegaret, Malwenn Lassudrie, Amélie Derrien, Aouregan Terre-Terrillon, Tomé Delaire, Caroline Fabioux

Comparative study of domoic acid accumulation, isomer content and associated digestive subcellular processes in five marine invertebrate species

José Luis García-Corona[1], Hélène Hegaret[1], Malwenn Lassudrie[2], Amélie Derrien[2], Aouregan Terre-Terrillon[2], Tomé Delaire[1], Caroline Fabioux[1]*

[1] Laboratoire des Sciences de l'Environnement Marin, UMR 6539 LEMAR (UBO/CNRS/IRD/Ifremer). Institut Universitaire Européen de la Mer, rue Dumont d'Urville, Technopôle Brest-Iroise, 29280 Plouzané, France.

[2]Ifremer, LITTORAL LER BO, Station de Biologie Marine, Place de la Croix, BP 40537, 29900 Concarneau Cedex, France.

*Corresponding author: Caroline Fabioux

Laboratoire des Sciences de l'Environnement Marin, UMR 6539 (CNRS/UBO/IFREMER/IRD). Institut Universitaire Européen de la Mer, Technopôle Brest-Iroise 29280, Plouzané, France.

e-mail: caroline.fabioux@univ-brest.fr

Abstract

Despite the deleterious effects of the phycotoxin domoic acid (DA) on human health, and the permanent threat of blooms of the toxic *Pseudo-nitzschia* sp. over commercially important fishery-resources, knowledge regarding the physiological mechanisms behind the profound differences in accumulation and depuration of this toxin in contaminated invertebrates remain very scarce. In this work, a comparative analysis of accumulation, isomer content, and subcellular localization of DA in different invertebrate species was performed. Samples of scallops *Pecten maximus* and *Aequipecten opercularis*, clams *Donax trunculus*, slippersnails *Crepidula fornicata*, and seasquirts *Asterocarpa* sp. were collected after blooms of the same concentration of toxic *Pseudo-nitzschia australis.* Differences (P <0.05) in DA accumulation were found, wherein *P. maximus* showed up to 20-fold more DA in the digestive gland than the other species. Similar profiles of DA isomers were found between *P. maximus* and *A. opercularis*, whereas *C. fornicata* was the species with the highest biotransformation rate (~10%) and *D. trunculus* the lowest (~4%). DA localization by immunohistochemical analysis revealed differences (P <0.05) between species: in *P. maximus*, DA was detected mainly within autophagosome-like vesicles in the cytoplasm of digestive cells, while in *A. opercularis* and *C. fornicata* significant DA immunoreactivity was found in post-autophagy residual bodies. A slight DA staining was found free within the cytoplasm of the digestive cells of *D. trunculus* and *Asterocarpa* sp. The Principal Component Analysis revealed similarities between pectinids, and a clear distinction of the rest of the species based on their capacities to accumulate, biotransform, and distribute the toxin within their tissues. These findings contribute to improve the understanding of the inter-specific differences concerning the contamination-decontamination kinetics and the fate of DA in invertebrate species.

Keywords: domoic acid, shellfish, DA isomers, autophagy, interspecific differences.

1. Introduction

Domoic acid (DA) is an extremely dangerous phycotoxin responsible of the illness referred as amnesic shellfish poisoning (ASP) syndrome in humans (Perl *et al.*, 1990, Pulido, 2008; La Barre *et al.*, 2014). This highly potent neuroexcitatory amino acid is naturally produced by some diatoms of the genus *Pseudo-nitzschia* (Bates *et al.*, 1998, 2018), wherein the species *Pseudo-nitzschia australis* is one of the most toxigenic (Lelong *et al.*, 2012; La Barre *et al.*, 2014). The recurrent presence of toxic blooms of *Pseudo-nitzschia* sp., and the subsequent production of DA, frequently affect fishery resources on the North Atlantic coasts of France. Indeed, suspension-feeding invertebrates are capable of ingesting toxic *Pseudo-nitzschia* cells leading to high amounts of DA accumulated in their tissues (Basti *et al.*, 2018; Dusek Jennings *et al.*, 2020) seriously threatening human health through contaminated seafood consumption (Pulido, 2008; La Barre *et al.*, 2014). Over the last two decades, these blooms have caused numerous and persistent harvest closures for some economically important species (Amzil *et al.*, 2001; Husson *et al.*, 2016).

Notwithstanding, profound inter-specific variability in the toxicokinetics of accumulation and depuration rates of DA burdens have been reported between several invertebrate species in the same affected area (Costa *et al.*, 2004, 2005a,b; Bogan *et al.*, 2007a,b,c; Lage et al., 2012; Ben haddouch *et al.*, 2016; Dusek Jennings *et al.*, 2020; Blanco *et al.*, 2021; Kvrgić *et al.*, 2022). Thus, invertebrates have been broadly classified as "fast" or "slow" DA-depurators (Blanco *et al.*, 2002a,b; Basti *et al.*, 2018). Larger scallops, such as King scallops *Pecten maximus* (Blanco *et al.*, 2002a; García-Corona *et al.*, 2022) and giant scallops *Placopecten magellanicus* (Gilgan, 1990; Haya *et al.*, 1991), some big-clams, such as razor clams *Siliqua patula* (Horner *et al.*, 1993; Dusek Jennings *et al.*, 2020), and some cephalopod mollusk such as *Octopus vulgaris* (Costa *et al.*, 2004) and *Eledone moschata* (Costa *et al.*, 2005b) as well as the common cuttlefish *Sepia officinalis* (Costa *et al.*, 2005a; Ben haddouch *et al.*, 2015) are capable of accumulating high amounts of DA, principally in the digestive gland, and require from many months to a couple of years to depurate the toxin from their tissues. Therefore, these species have been considered as slow DA-depurators. Notwithstanding, during *Pseudo-nitzschia* outbreaks, the king scallop *P. maximus* is usually amongst the most contaminated species (James *et al.*, 2005; Blanco *et al.*, 2002a, 2021). Levels of DA exceeding up to 5-fold the European regulatory limit of 20 mg kg^{-1} are not unusual in *P. maximus* (Blanco *et al.*,2006; Bogan *et al.*, 2007a,b; García-Corona *et al.*, 2022). Conversely, mussels (Novaczek *et al.*, 1992 ; Blanco *et al.*, 2002b; Mafra *et al.*, 2010), and even smaller scallops, such as

Argopecten purpuratus (Álvarez *et al.,* 2020) are known as fast DA-depurators since they can depurate up to 90 % of total DA burdens over hours to days. These species-specific differences in DA accumulation-depuration represent a real issue for fishery economy and management after ASP-blooms. Thus, understanding the physiological mechanisms behind this phenomenon is of high interest.

Mauriz and Blanco (2010), as well as Lage *et al.* (2012) found that nearly 90% of total DA accumulated in *P. maximus* and *O. vulgaris*, respectively, was free in a soluble form in the cytoplasm of the digestive cells. García-Corona *et al.* (2022) observed, using an immunohistochemical subcellular localization of DA in *P. maximus,* that DA is trapped into small-spherical membrane-bound vesicles localized in the cytoplasm of digestive cells, suggesting that autophagy could be one of the potential physiological mechanisms behind the long retention of a part of DA in this species. Nevertheless, to date, the immunohistochemical (IHC) localization of DA has not been applied to any other invertebrate species contaminated with DA, which greatly hinders the comparison of the subcellular mechanisms involved in the accumulation and retention of this toxin between affected species. Autophagy is a highly regulated and dynamic "self-eating" catabolic system related to the intracellular ingestion and digestion (Cuervo, 2004; Wang *et al.,* 2019; Zhao *et al.,* 2021). Through autophagy the lysosomes receive autophagosomic vesicles (autophagosomes) containing cytoplasmic cellular components, such as macromolecules, damaged or misfolded proteins, and entire organelles, as well as extracellular-derived molecular cargo from endocytosis and phagocytosis for degradation, digestion, recycling, or excretion (Klionsky *et al.,* 2014; McMillan, 2018; Wang *et al.,* 2019). These distinctive capabilities establish an essential role of autophagy in maintaining metabolic homeostasis and cellular health in bivalves (Balbi *et al.,* 2018; Picot *et al.,* 2019; Rodríguez-Jaramillo *et al.,* 2022).

Not only untransformed DA, but also some structural isomers of the toxin (*i.e.* isoA, isoD, isoE, and epi-DA) are frequently detected in seafood during ASP-monitoring. The concentrations of DA-isomers commonly range from 0.5 to ~20% of total DA burdens (Wright *et al.,* 1990a; Costa *et al.,* 2005; Takata *et al.,* 2009; Zheng *et al.,* 2022). Despite some studies pointing out some degree of species-specific biotransformation of DA in bivalves (Wright *et al.,* 1990b; Blanco *et al.,* 2010), fish and shellfish (Vale and Sampayo, 2001), and cephalopods (Costa *et al.,* 2005), no work has ever compared the biotransformation profiles of DA against the subcellular localization of this toxin in contaminated invertebrates. This information could be useful to elucidate differences in DA

uptake and allocation, as well as the potential implication of subcellular mechanisms on depuration of this toxin between species.

This study compared biotransformation and subcellular localization of DA in five invertebrate species simultaneously exposed to natural toxic *P. australis* blooms to answer the question: How do invertebrate species differ in their ability to accumulate, process, and allocate DA in their tissues?

2. Materials and methods

2.1. Sample collection and *Pseudo-nitzschia australis* bloom-associated environmental data

A total of 38 invertebrate samples were collected in 2021 in the northwest coast of Brittany, France. The samples consisted in clams *Donax trunculus* (n =11) collected on the 30th of March in the Bay of Douarnenez, and scallops *P. maximus* (n =5), *A. opercularis* (n =10), slippersnail *Crepidula fornicata* (n =7), and sea squirt *Asterocarpa sp.* (n =5) collected on the 8th of April in Camaret-sur-Mer (Fig. 1). Animals were collected eight days after blooms of similar intensity of the DA-producing *P. australis* according to the French national phytopankton monitoring network (French Observation and Monitoring program for Phytoplankton and Hydrology in coastal waters, REPHY) in both sampling sites ([2.6×10^5 cell.L^{-1}] on March 23, 2021 in the Bay of Douarnenez), and [1.1×10^5 cell.L^{-1}] on March 30, 2021 (in Camaret-sur-Mer), respectively, https://bulletinrephytox.fr/accueil) (Fig 1). Once at the laboratory, the digestive gland (DG) of the scallops (*P. maximus* and *A. opercularis*) was carefully dissected from the rest of the tissues, and subsequently sectioned in two halves. For the rest of the species with diffuse visceral mass (*C. fornicata*, *D. trunculus*, and *Asterocarpa* sp.) the soft body (*i.e.* total flesh) was divided into two equal portions at the mid visceral level, including a section of the DG on each. For each individual, one of these DG/visceral sections was fixed in Davidson's solution (Kim *et al.*, 2006) for histology, and the second DG/visceral sections section was stored at -20 °C for toxin analysis.

2.2. Toxin quantification and DA-isomer analysis by liquid chromatography-tandem mass spectrometry (LC-MS/MS)

Since the DG accumulates most of DA (Mauriz and Blanco, 2010), only this tissue was considered for toxin analysis in this work. For the non-pectinid species, the DG was separated

from the rest of the visceral mass once the tissues were frozen. DA was extracted from the DG following the procedure described by Quilliam *et al.*, (1989). Samples were homogenized from 200 ± 10 mg of frozen DG in 1 mL of 50% MeOH/H_2O using a Fastprep-24 5G system (MP Biomedicals, Sta. Ana, CA, USA). The extract was clarified by centrifugation at 19,000 × g at 4 °C for 10 min and the supernatant was isolated, filtered through a 0.2 µm nylon centrifugal filter (VWR International, Radnor, PA, USA), and stored at -20 °C until analysis.

The quantification of total DA (tDA = ensemble of all DA isomers) and each isomer of the toxin in the DG was carried out by LC-MS/MS according to Ayache *et al.* (2019) with modifications, using a Shimadzu UFLCxr system coupled to a quadruple hybrid mass spectrometer API400Q-Trap (Sciex, Concord, ON, Canada) equipped with a heated electrospray ionization (ESI) source. Chromatographic separation was carried out on a reversed-phase column Phenomenex Luna Omega C18 (150 × 2.1 mm, 3 µm, Phenomenex, Torrance, CA, USA). The separation was carried out using a mobile phase consisting of aqueous eluent A (100% H_2O + 0.1% H-COOH) and organic eluent B (95% CH_3CN/ 5% H_2O + 0.1% H-COOH). The run started following a gradient from A to B as follows: 5% at min 0, 18.6% at 17 min, 95% at 17.5 min, 95% at 19.5 min, 5% at 20 min, and 5% at 25 min. The flow rate was 200 $\mu L.min^{-1}$ and the injection volume was 5 µL. The column temperature was maintained at 30 °C.

The ESI interface was operated with a curtain gas of 20 psi, temperature of 550 °C, gas1 55 psi, gas2 60psi, and an ion spray voltage of 5500 V. The detection of DA was achieved by multiple reaction monitoring (MRM) in positive ion mode. The transition 312.1 > 266.1 (collision energy = 22 V) was used for quantification and 312.1 > 161.1 (collision energy = 33 V) for confirmation. The quantification was performed relative to the DA standard (National Research Council Canada, NRCC) with a 6-point calibration curve. The Limit of Quantification (LOQ) (S/N = 10) and the Limit of Detection (LOD) (S/N = 3) of the method were 0.25 and 0.08 ng DA mL^{-1}, respectively, which corresponded to 1.25 and 0.4 ng DA g^{-1} in tissue.

2.3. Immunodetection of DA and quantitative histology

Tissue samples fixed in Davidson's solution were dehydrated in ethanol series of progressive concentrations (70%, 80%, 95%, and 100%), cleared in xylene, and embedded in paraffin (Paraplast Plus, Leica Bio-systems, Richmond, IL, USA). Paraffin blocks were cut in 4-µm-thick sections using a rotary microtome (Leica RM 2155, Leica Microsystems) and sections

mounted on polylysine-coated glass slides (Sigma-Aldrich, St. Louis, MO, USA). A series of three consecutive sections was performed for each sample, which were used for (i) immunohistochemical detection of DA, (ii) multichromic staining, and (iii) hematoxylin/eosin staining, as described below. Sections were deparaffinized in xylene and rehydrated in ethanol series of regressive concentrations before staining.

In order to detect the presence of DA at the subcellular level in the tissue sections, an immunohistochemical DA labeling technique was applied following the procedure described in García-Corona *et al.* (2022) on the first slide of each sample. Briefly, tissue sections were incubated overnight with a Goat polyclonal anti-DA primary antibody (0.01 $mg.mL^{-1}$, Eurofins Abraxis®, Warminster, PA, USA) at 4°C, and the next day the slides were incubated at 37 °C for 2h with an HRP sharped IgG Rabbit anti-Goat secondary antibody (0.001 $mg.mL^{-1}$, abcam®, Cambridge, UK). Then, samples were washed and revealed with diaminobenzidine (DAB+ Chromogen Substrate Kit, abcam®, Cambridge, UK) for 1 h in darkness at room temperature and counterstained with Harry's hematoxylin.

The second slide from each sample was stained with a multichromic procedure (Costa and Costa, 2012). This technique consists of a combination of Alcian Blue and Periodic Acid–Schiff's for the demonstration of acid mucopolysaccharides and neutral glycoconjugates, in blue and magenta tones, respectively, Hematoxylin blueing for nuclear materials, and Picric Acid to identify proteins in yellow hues.

The last set of tissue sections was stained with Hematoxylin–Eosin as reference (Kim *et al.*, 2006). The slides were examined under a Zeiss Axio Observer Z1 light microscope.

For quantitative histological analysis, five randomly selected regions (63×; ~1.3 mm^2) from each DG section treated for immunohistochemical DA detection, multichromic, and hematoxylin-eosin staining were digitized at high resolution (600 dpi). A total of 570 images (*i.e.* 114 micrographs by species) were used to obtain the following data: (a) DA chromogenic signal (DAcs) corresponds to the coverage area, in pixels, occupied by the positive anti-DA staining. This was manually calculated using an operator-driven digital image analysis system (Image Pro Plus software v. 4.5, Media Cybernetics, Silver Spring, MD, USA) (Gómez-Robles *et al.*, 2005). The area reported as the DA chromogenic signal was calculated as DAcs = (DA chromogenic signal area/ total area occupied by the DG on the analyzed region of the slide) × 100. Since almost all the DA chromogenic signal detected in DG is trapped in membrane-bound vesicles present in the cytoplasm of digestive cells (García-Corona *et al.*,

2022), the (b) Total autophagy (Ta) and total DA autophagy (DAa) were calculated by counting the total number of autophagosome-like vesicles, and the number of autophagosome-like vesicles with DA chromogenic signal, respectively, on each digitized image. A fraction of the DA chromogenic signal is also observed in post-autophagic residual bodies within the digestive cells (García-Corona *et al.*, 2022), thus the frequencies of (c) Total residual bodies (Trb) and DA residual bodies (DArb) were assessed as the total number of residual bodies and the total number of residual bodies with DA chromogenic signal, respectively, on each digitized image. Finally, (d) Cell vacuolization (Vac), measured as an indicator of potential histopathologies related to DA accumulation in the DG, represents the total number of vacuoles within the digestive cells of each invertebrate species on each digitized image.

2.4. Statistical analysis

All statistical analyses were performed in the R computing environment (R v. 4.2.2, R Core Team, 2022). *A priori* Lilliefors (Kolmogorov-Smirnov) and Bartlett tests were applied to confirm the normality of frequencies and homogeneity of variances of the residuals of the data, respectively (Hector, 2015). All data were transformed (log, $1/\chi$, or $\sqrt{\chi}$) prior to analysis to meet a priori assumptions. The percentage-expressed values were also arcsine (arcsine $\sqrt{P}$) transformed (Zar, 2010), but all data are reported untransformed as the means ± standard errors (SE). Separate one-way analyses of variance (ANOVA, type II Sum of Squares) were applied to assess statistically significant differences of toxin accumulation in the DG, proportion of DA isomers, and quantitative histological features between species. As needed, post hoc comparisons of means with Tukey's honest significance test (HSD) were performed to identify differences between means (Hector, 2015; Zar, 2010). Principal component analysis (PCA) was performed using the FactoMineR package with the factoextra package for data visualization into smaller factorial clusters within a 95% confidence interval. All data matrices were auto-scaled before PCA analysis. The corrplot package was run to calculate the correlation coefficients and their significance between variables within their given PCs. All graphics were generated using the package ggplot2. The level of statistical significance was set at $\alpha = 0.05$ for all analyses (Zar, 2010).

3. Results

3.1. Toxin accumulation and biotransformation

Significant differences in the amounts of total DA (tDA) accumulated in the digestive glands (DG) were found between the different invertebrate species sampled after blooms of the toxic *P. australis* (Fig. 2). The significantly higher burdens of tDA were observed in the scallop *P. maximus*, with 638.6 ± 35.5 mg.kg^{-1}, followed by those of the snail *C. fornicata*, with 48.5 ± 14.2 mg.kg^{-1}, the scallop *A. opercularis* (22.7 ± 2.6 mg kg^{-1}), and the clam *D. trunculus* (12 ± 1.7 mg kg^{-1})., The lowest values (P <0.05) of tDA were found in the ascidian *Asterocarpa* sp. (4.2 ± 1.5 mg kg^{-1}). Moreover, as shown in Fig. 2, an important intraspecific variability in tDA accumulation was also observed in *P. maximus* and *C. fornicata*, with values ranging from 530 to 731 mg kg^{-1}, and from 0.2 to 93.8 mg kg^{-1}, respectively.

The toxin analysis carried out by LC-MS/MS revealed differences in biotransformation of DA in the digestive glands among the different invertebrate species (Table I). For all species, relative concentration levels of DA isomers were <10 % of the tDA burdens. Nonetheless, *C. fornicata* was the species with the highest proportions (P <0.001) of DA isomers (9.3 ± 1.1 %), while *D. trunculus* showed significantly low DA isomer amounts (4.2 ± 0.3 %). Concerning the analysis of DA isomers proportion, *P. maximus* and *A. opercularis* showed similar biotransformation profiles of the toxin since similar amounts of each DA isomer were reported in both species. Furthermore, as shown in Table I, among the five species, the lowest ratio of isoE (P <0.05) was measured in *Asterocarpa* sp., and a significantly higher proportion of isoD was recorded in *C. fornicata*, while the smallest amounts (P <0.05) of isoA and epi-DA were quantified in *D. trunculus*.

3.2. DA subcellular localization and histological measurements

The microanatomical observations of histological sections evidenced qualitative differences in the localization of DA and the subcellular features linked to the accumulation of the toxin among the invertebrate species analyzed in this study (Fig. 3, and supplementary materials S1-5). DA detected by immunohistochemistry (IHC) appeared as a brown chromogenic signal (cs) on slides (Fig 3A, 3D, 3G, 3J, 3M, and S1A-B, S2A-B, S3A-B, S4A-B, S5A-B).

In the digestive gland of *P. maximus* DA was detected mainly trapped within small (~1-2.5 µm diameter) autophagosome-like vesicles (a) distributed throughout the cytoplasm of the digestive cells (dc). A narrow fraction of DA-immunoreactivity was also observed in residual bodies (rb) distributed in the acinar region (ar) of the digestive diverticula (dd) (Fig. 3A, S1A-B). The presence of membrane-bounded vesicles (a) with positive DA-signal (cs) in the

tubular region (tr) of the digestive diverticula (dd) was confirmed by means of the multichromic staining (MC), which produces a dark violet/blue hueing in membrane-bounded structures (Fig. 3B, S1C-D). Hematoxylin-Eosin (H&E) staining (Fig. 3C, S1E-F) highlighted a moderate vacuolization (v) within the cytoplasm of the digestive cells of *P. maximus*. Neither the autophagosomes (a) nor the residual bodies (rb) acquired any coloration with the H&E staining but residual bodies appeared yellow-green.

In the queen scallop *A. opercularis*, a strong DA-chromogenic signal (cs) was found in the residual bodies (rb) of the digestive diverticula (dd) (Fig. 3D, S2A-B). No DA chromogenic signal was observed in the autophagosome-like vesicles (a) present in the cytoplasm of the digestive cells of the digestive diverticula (dd) (Fig. 3E-F, S2A-B). An intense process of vacuolization (v) of the digestive cells of *A. opercularis* was found (Fig. 3E-F, S2C-D), while H&E staining (Fig. 3F, S2E-F) showed that the autophagosomes seem to gather giving rise to the residual bodies (rb) in the cytoplasm of the adipocyte-like digestive cells (al) of the digestive diverticula (dd).

A similar result was found for *C. fornicata*, since most of the brown DA-chromogenic staining (cs) was found in small residual bodies (rb) present in the basal cytoplasmic region (bl) of the digestive cells (dc) (Fig. 3G, S3A-B), while autophagosome-like vesicles (a) that are distributed in the apical region of the digestive cells (dc) (Fig. 3H-I, S3A-B) did not show any DA-immunoreactivity.

A slight-blurred DA-chromogenic signal (cs) was also observed only free in the cytoplasm of the digestive cells of *D. trunculus* (Fig 3J, S4A-B). The presence of autophagosome-like vesicles (a, small blue colored vesicles distributed in the cytoplasm, Fig 3K, S4C-D) and residual bodies (rb, larger round non-colored structures present within adipocyte-like cells, Fig 3L, S4C-D) was confirmed in the digestive cells (dc) of clams (Fig. 3K-L, S4C-F).

Meanwhile, in sea squirts (*Asterocarpa* sp.) DA-chromogenic signal (cs) was rarely identified and was located as small brown points (Fig. 3M, S5A-B) distributed through the digestive epithelium (pse) of the blind ampulla (ba) (Fig. 3N-O, S5C-F).

The results of the quantitative analysis of histological parameters are shown in Fig. 4. The coverage area of the DA chromogenic signal (%DAcs, Fig. 4A) was significantly higher in the most contaminated invertebrate species (*P. maximus* = 4.8 ± 0.4 %, and *C. fornicata* = 5.3 ± 0.4 %). In addition, differences ($P < 0.05$) were found in the amount of DA chromogenic

signal in *A. opercularis* (3.2 ± 0.2 %) compared to the species contaminated with the lowest DA burdens (*D. trunculus* = 0.2 %, and *Asterocarpa* sp. = 0%).

On the other hand, as seen in Fig. 4B, total autophagy (Ta) reached its highest values (P <0.05) in the bivalve species, with frequencies of 185.4 ± 18 autophagosomes. area^{-1} in *P. maximus*, 123.2 ± 12.6 autophagosomes. area^{-1} in *D. trunculus*, and 102.9 ± 9.7 autophagosomes. area^{-1} in *A. opercularis*. The proportion of total autophagy (Ta) was significantly lower in *C. fornicata* (60.9 ± 5.8 autophagosomes. area^{-1}) and *Asterocarpa* sp. (18.3 ± 2.9 autophagosomes. area^{-1}). Nevertheless, the frequency of autophagosomes with positive DA-chromogenic signal (DAa) significantly peaked in *P. maximus* (99.7 ± 9.7 autophagosomes. area^{-1}, corresponding to 53.8% of the Ta), followed by *C. fornicata* (39.8 ± 4.6 autophagosomes. area^{-1}, corresponding to 65.3% of the Ta). The lowest proportions (P <0.05) of autophagosomes with positive DA-chromogenic signal (DAa) were observed in *A. opercularis*, *D. trunculus*, and *Asterocarpa sp*, with ≤7 autophagosomes. area^{-1}, which corresponded to 8.4, 1.2, and 0% of the total autophagy (Ta), respectively (Fig. 4B). In contrast, the frequencies of total residual bodies (Trb) and residual bodies with DA chromogenic signal (DArb) significantly peaked in *C. fornicata* (92.4 ± 5.2 rb. area^{-1}, and 51.9 ± 4.1 rb. area^{-1}, respectively), while the frequencies of both subcellular parameters showed their lowest values (P <0.05) in the rest of the species (Fig. 4C). It is important to highlight that the percentage of residual bodies with DA chromogenic signal (%DArb) compared to total residual bodies (Trb) was significantly higher in *A. opercularis*, with a 67.1 ± 3%, followed by *C. fornicata* and *P. maximus*, with rates of 58 ± 3.8% and 35.4 ± 3.3%, respectively. The lowest % DArb (P <0.05) was reported for *D. trunculus* (2.2 ± 1.3%) and *Asterocarpa sp.* (0%). Finally, the highest frequency of cell vacuolization (Vac) of the digestive cells was measured in *A. opercularis* (67.4 ± 6.7 vacuoles. area^{-1}, P <0.05), followed by *P. maximus* (31.6 ± 2.4 vacuoles. area^{-1}). Significantly lower vacuolization (Vac) rates were reported for the rest of the species (<8 vacuoles. area^{-1}, Fig. 4D).

3.3. Integrative analysis compiling DA accumulation/biotransformation and subcellular features

A principal component analysis (PCA) was computed to summarize all variables measured in this study on the five invertebrate species studied: DA accumulation, biotransformation, and subcellular parameters (Fig. 5). The PCA described two-thirds (66.6 %) of the total variance of the data along the first two principal dimensions. For the whole data set, the clustering-

PCA provided a clear distinction between species, except for the two pectinid species, which slightly overlapped (Fig. 5A). In the scatter plot, *P. maximus* and *A. opercularis* showed similar scores on the principal components and were different from the rest of the species. Meanwhile, *D. trunculus*, *C. fornicata,* and *Asterocarpa* sp., were grouped separately from each other (Fig. 5A). As shown in Fig. 5B, the dimension/principal component 1 (PC1, 42.3 % of the total variance) mainly explained the accumulated untransformed DA, isoD and isoA, as well as the histological parameters such as domoic acid chromogenic signal (%DAcs), domoic acid autophagy (DAa), total residual bodies (Trb), and residual bodies with DA signal (DArb). In this PC1, the fraction of isoA was strongly and positively correlated to the %DAcs and DArb (r = 0.5 and 0.6, P <0.05, respectively). Likewise, a strong and significant correlation was found between the untransformed DA and DAa (r = 0.8), and between DArb and %DAcs (r = 0.8) in this dimension. The amounts of isoE and epi-DA, as well as total autophagy (Ta) and vacuolization (Vac), were the strongest correlated variables to dimension/principal component 2 (24.3 % of the explained variance). A positive correlation (r = 0.5, P <0.05) between total DA (tDA) and isoE was found with Ta within the PC2. As observed in Fig. 5, *P. maximus* and *A. opercularis* were associated with higher tDA and isoE, as well as the maximum frequencies of Ta and Vac. Meanwhile, *C. fornicata* was related to higher amounts of isoD, epi-DA, Trb, and *D. trunculus* with the highest fraction of untransformed DA.

4. Discussion

In this study, we compared domoic acid (DA) accumulation and isomer profiles with the subcellular localization of this toxin among naturally contaminated invertebrates to progress in the understanding of interspecific differences in DA fate in marine invertebrates.

The DA contents measured in invertebrate tissues are the result of the accumulated and the subsequently depurated toxin. Moreover, differences in DA accumulation in the organisms are strongly dependent on the toxicity of the *Pseudo-nitzschia* cells, the duration of the ASP blooms, the time through the animals were exposed to toxic microalgae, and the moment at which the organisms were sampled during the bloom. In this work, DA contaminated animals were collected 8 days after maximum cell densities of *P. australis* bloom of similar intensity, duration and origin.

Since DA is a highly water-soluble molecule, it is expected to be easily accumulated in the majority of forager species (Trainer *et al.,* 2012; La Barre *et al.,* 2014). Nonetheless, the scallops, but notably *P. maximus*, as well as *C. fornicata,* remained significantly more contaminated than the rest of the species in this study. These important differences in DA accumulation in the digestive gland at the interspecific level are in accordance with considerably high variability in DA amounts frequently detected in these species (Bogan *et al.,* 2007a,b,c; Basti *et al.,* 2018, Blanco *et al.,* 2021) resulting from differences in the accumulation but also in the depuration rates of DA reported mostly for bivalve species (Vale and Sampayo, 2001; Blanco *et al.,* 2010; Dusek Jennings *et al.,* 2020). Notably, within the pectinidae family, some large scallops like *P. maximus* can accumulate up to 3,200 mg $DA.kg^{-1}$ in their DG (James *et al.,* 2005; Blanco *et al.,* 2006), which is 5-fold more than the DA accumulated in the DG of the same species in this work. In contrast, smaller scallops, such as *A. opercularis* (Ventoso *et al.,* 2019), *A. purpuratus* (Álvarez *et al.,* 2020) and *A. irradians* (O'Dea *et al.,* 2012) accumulate lower DA burdens (~7-30 mg $DA.kg^{-1}$) similar to those recorded in *A. opercularis* in this work, in the same organs. Depuration kinetics of the toxin differ also between these species. Whereas *P. maximus* exhibits depuration rates as slow as 0.007 day^{-1} in the DG, remaining highly contaminated for months or even a few years (Blanco *et al.*, 2002a, 2006), other scallops such as *A. purpuratus* show decontamination debits near to 10 day^{-1} in the DG, allowing to depurate ~90% of total DA burdens within hours or a couple of days (Álvarez *et al.*, 2020). Thus, after all the differences in accumulation and depuration rates of DA between invertebrate species discussed above, a possible event of rapid depuration of DA in *A. opercularis*, *D. trunculus,* and *Asterocarpa* sp. before sampling can be part of the interspecific differences of DA concentrations measured in this study. Several factors could explain variability in DA decontamination: the transfer of DA in other tissues than DG, its biotransformation and its depuration.

Differential tissue distribution of DA may not explain more than 20% of the interspecific variability observed in this study since the digestive gland accumulates more than 80% of total DA burdens in most invertebrates (Blanco *et al.,* 2002a; Costa *et al.,* 2005a,b). For all the five species of this study, three bivalve molluscs *(P. maximus*, *A. opercularis* and *D. trunculus*), one gasteropod mollusc (*C. fornicata*) and one ascidian (*Asterocarpa* sp.) DA isomers were observed in digestive gland with significant interspecific differences between the proportions of isomers E, D, A and epi-DA; iso-E being more represented in molluscs compared to ascidian. Although it is known that DA isomerization can occur within toxic

Pseudo-nitzschia cells (Amzil *et al.,* 2001; Bates *et al.,* 2018; Quilliam *et al.,* 1989; Wright *et al.,* 1990a), in the present study all invertebrate species were exposed to the same *Pseudo-nitzschia* toxic bloom. These two sets of information demonstrate that metabolic conversion of DA occurs in marine invertebrates as hypothesized first by Vale and Sampayo (2001) and is species-specific. The integrative analysis revealed a close and significant relationship between some subcellular features (vacuolization, autophagy, presence of residual bodies) and the isomer profile of the toxin. Understanding DA compositional changes is important not only as a means of predicting toxicity, but also because biotransformation could participate in the prolonged retention of this toxin in invertebrate species by means of some of the subcellular mechanisms analyzed here. Notwithstanding, biotransformation does not appear to be the main route of DA elimination in these species since it represents less than 10% of total DA of the digestive gland measured in these five species, as well as in previous studies (Costa *et al.,* 2005a; Blanco *et al.,* 2010; Zheng *et al.,* 2022). There is only one study showing some insights of DA biotransformation linked to apparent augmentation of the overall DA detoxification rate in the cuttlefish *Sepia officinalis*, wherein DA isomers comprise a relevant percentage of the toxin profile in the branchial hearts, suggesting that this organ has an important function in system detoxification of DA (Costa *et al.,* 2005a).

Furthermore, it is worth to mention that king scallops were slightly contaminated (~5 mg DA kg^{-1}, data from the REPHY French monitoring program) before the bloom of *P. australis* occurred in late March 2021, after which they became highly contaminated (~ 650 mg DA kg^{-1}). Therefore, it is inferred that the concentrations of DA isomers found in the digestive glands of *P. maximus*, and consequently, in all the invertebrate species analyzed in this work, were the result of the bloom of *P. australis* occurred in late March 2021.

Despite the enormous differences in DA concentrations between the marine invertebrates analyzed in this work, the physiological mechanisms behind this phenomenon remain poorly understood. To date, only a few hypotheses about the biological processes potentially involved in the large accumulation and long retention of DA in some bivalve species have been proposed. On the one hand, Trainer and Bill (2004) characterized tissue-specific expression of high and low affinity glutamate receptors in *S. patula*, inferring that this species might selectively express low affinity glutamate receptors in all tissues, and high affinity sites in specific tissues that retained DA for long periods of time. On another hand, Mauriz and Blanco (2010) hypothesized that one of the causes of the long retention of DA in the DG of *P. maximus* was not the binding of the toxin to some cellular component as previously discussed,

but the lack of efficient membrane transporters in the scallops to excrete the toxin. Recently, using immunostaining of DA, García-Corona *et al.* (2022) revealed that in *P. maximus,* once entered the cells, a part of DA was localized in the cytoplasm of digestive cells of the digestive diverticula, trapped within autophagosome-like vesicles. Moreover, transcriptomic analyses revealed the upregulation of genes related to autophagy and vesicle-mediated transport in the DG of *P. maximus* injected with DA in the adductor muscle (Ventoso *et al.*, 2021), as well as in the DG of *A. opercularis* after exposure to DA-producing *Pseudo-nitzschia* (Ventoso *et al.*, 2019). Taken together, these data suggest that the formation of autophagosomal structures could be part of the explanation for the long retention of DA in *P. maximus*. The results obtained in this work cope with these findings, since most of the DA-labeling was found within a large number of autophagosomes distributed throughout the cytoplasm of the digestive cells in *P. maximus.* Additionally, a strong DA-chromogenic signal was found within the post-autophagic residual bodies present in the adipocyte-like cells in *A. opercularis,* and in the basal region of the digestive diverticula in *C. fornicata*. During autophagy the lysosomes in the digestive cells of these species receive DA trapped within autophagosomic-vesicles. Nonetheless, the evidence of this work indicates that a fraction of DA remains accumulated within autophagosomic structures instead being excreted or used by the cells, leading to its accumulation within the autophagosomes, and consequently blocking its excretion outside the cell by exocytosis (Cuervo, 2004; Zhao *et al.*, 2021). This eventually triggers the aggregation of autophagosomes with sequestered DA to form residual bodies that can remain in the cytoplasm of the digestive cells indefinitely. There is evidence of the long retention of exogenous compounds through specialized cellular mechanisms in animals. A concrete example is the dynamics of phagocytosis displayed by dermal macrophages, explaining both persistence and strenuous removal of tattoo ink in mammalian skin. Baranska *et al.* (2018) demonstrated that upon tattooing, pigment particles are captured by dermal macrophages. Eventually, macrophages laden with tattoo ink die and release the pigment particles, which remain in an extracellular form at the site of tattooing where they are recaptured by neighboring or incoming macrophages. Through adult life, several cycles of ink capture-release-recapture can occur, accounting for long-term tattoo persistence (Baranska *et al.*, 2018). Macrophagy and autophagy are analogous processes. During macrophagy specialized cells called macrophages use their cytoplasmic membranes to engulf large extracellular particles (≥ 0.5 µm, *i.e.* bacteria and debris) via endocytosis, giving rise to internal vesicular

compartments called phagosomes. Phagosomes with cargo materials fuse with lysosomes, forming phagolysosomes, leading to enzymatic degradation (Flannagan *et al.*, 2012; Gordon, 2016). Like autophagy, macrophagy is a major mechanism used to remove pathogens and cellular debris for detoxification or nutrient recycling purposes, in which macrophages can have lifespans of months to a few years (Baranska *et al.*, 2018). The discussion above raises a new hypothesis suggesting that a part of DA that is not excreted from the cells due to the lack of efficient membrane transporter (Mauriz and Blanco, 2010), may undergo successive cycles of capture–release–recapture by autophagosomes through the regenerative cycle of digestive cells in some invertebrates, without any or very few toxin vanishing from months to years. Therefore, long-term DA persistence could rely on autophagosome renewal or on potential longevity of residual bodies. A close relationship between early autophagy and DA sequestration can be established in *P. maximus*, whereas in *A. opercularis* and *C. fornicata* toxin accumulation seems to be closely linked to late autophagy and the formation of residual bodies in the DG. This evidence strengthens the hypothesis stated by García-Corona *et al*. (2022), where autophagy was proposed as one of the possible causes of the prolonged retention of part of DA initially accumulated, now not only in *P. maximus*, but also in other marine invertebrates. The next step is to decipher the fate and life-spent of autophagosomes and residual bodies with anti-DA immunolabelling within a scenario of contamination and decontamination.

Although the IHC method for the *in situ* detection of DA in contaminated invertebrates used in this work has a high-sensitivity (~1 mg DA.kg^{-1}, García-Corona *et al.*, 2022) only a slight-blurred DA chromogenic signal was found in the cytoplasm of the digestive cells of *D. trunculus*, and *Asterocarpa* sp. This would suggest that in these species, intracellular DA is not bound to any subcellular structure or component. Consequently, the feeble amounts of toxin free in the cytoplasm of the digestive cells could be quickly depurated after DA contamination but a part of DA, could also be lost by washing during histological process. Furthermore, when all species are compared, the proportion of DA chromogenic signal seems not correspond to the total amount of toxin accumulated in the DG of the animals. Despite the large difference in DA concentration between *P. maximus* and *A. opercularis* (638.6 mg DA kg^{-1} *vs* 22.7 mg DA kg^{-1}, respectively), the difference in DA signal was small (~2 % between both species). Therefore, it is possible that a fraction of the DA accumulated in the DG of both species is free and dissolved in the cytoplasm of the digestive cells as reported for *P. maximus* (Mauriz and Blanco, 2010) and for *O. vulgaris* (Lage *et al.*, 2012), and that *P.*

maximus effectively lacks efficient membrane transporters to excrete the toxin out of the cell (Mauriz and Blanco, 2010), thus the chromogenic signal observed in the DG of both pectinids could correspond to the fraction of DA trapped by the autophagic system, and not to the total DA burdens in the DG. Further analyzes will be necessary to corroborate all the ideas discussed above.

Scallops, *P. maximus* but even more so *A. opercularis* contaminated by DA in this study have significantly higher digestive cell vacuolization rates in their digestive gland compared to other species. Cell vacuolization is a common histopathological lesion in bivalves under stressful environmental conditions (Rodríguez-Jaramillo *et al.,* 2022). According to Shubin *et al.* (2016) this is a well-known subcellular phenomenon observed in animal cells which often accompanies cell death after exposure to artificial or natural low-molecular-weight compounds, such as DA. The scarce literature related to the effects of *Pseudo-nitzschia spp*. or DA on invertebrates indicates that DA could potentially disturb behavioral, metabolic, molecular, and physiological processes in some bivalves such as *P. maximus* (Ventoso *et al.*, 2021; Liu *et al.,* 2007a,b), *A. opercularis* (Ventoso *et al.,* 2019), *A. irradians* (Chi *et al.,* 2019), and some mussels, like *M. edulis* (Dizer *et al.,* 2001) and *M. galloprovinciallis* (Pazos *et al.,* 2017). Nevertheless, no lethal effects resulting from exposure to DA have been reported in any of these species, suggesting either a low sensitivity to the toxin or yet unnoticed negative effects. Further research is needed in order to decipher how DA exposure and its biotransformation modulate cell vacuolization, as well as its potential detrimental effects on the digestive cells of pectinids, and possibly, over other invertebrates, as reported for other phycotoxins in other bivalve species (Hegaret *et al.,* 2010; Lassudrie *et al.,* 2014).

Furthermore, as discussed above, the highest proportions of total autophagy, and production of residual bodies reported in *P. maximus*, *A. opercularis*, and *C. fornicata*, seems to directly correspond to the sequestration of DA within these subcellular structures, which indicates that autophagy could be also considered as a sign of homeostatic impairment, as reported in other marine bivalve species when activated as an auxiliary mechanism for recycling internal energy to cope with detrimental environmental conditions (Moore, 2008; Rodríguez-Jaramillo *et al.,* 2022), or to depurate toxicological agents (Moore, 2004; Picot *et al.,* 2019). The particularly highest proportions of DA-autophagy in *P. maximus* analyzed here stress out the need to carry out the measurement of the frequency of these subcellular features in a DA contamination and decontamination scenario. This basic knowledge is necessary to confirm

these physiological processes are the actual reasons for the long retention of a part of this toxin in this species.

The findings presented in this work put in evidence DA biotransformation in invertebrate species, and strongly suggest the role of subcellular mechanisms such as early and late autophagy, in the accumulation, localization and long retention of DA in some marine invertebrates.

5. Conclusions

The evidence presented in this work corroborates the profound interspecific differences in the accumulation of DA between different species of marine invertebrates, as well as species-specific profiles of toxin biotransformation among the analyzed species. Similar profiles of DA isomers were found between *P. maximus* and *A. opercularis*, whereas *C. fornicata* was the species with the highest biotransformation rate, and *D. trunculus* the lowest. In *P. maximus, A. opercularis* and *C. fornicata* the DA chromogenic signal was detected mainly within autophagosomic-structures in the cytoplasm of digestive cells, while in *D. trunculus* and *Asterocarpa* sp. DA signal was found free in the cytoplasm of the digestive cells. This evidence indicates that localization of DA and its effects at the subcellular level appear to be species-specific, and the integrative analysis revealed that these parameters could be potentially influenced by the biotransformation profiles of the toxin. All this new information is highly valuable to strengthen ASP-monitoring systems since most of the invertebrate species analyzed in this work could be used as sentinels of DA contamination in affected areas. Furthermore, this study provides a set of innovative histological parameters developed to assess quantitatively some subcellular mechanisms potentially involved in the accumulation and long-retention of DA among contaminated invertebrates. This quantitative information may be integrated into numerical models that allow estimating and predicting toxicokinetics of contamination and depuration in fishery-stocks frequently affected during blooms of toxic *Pseudo-nitzschia sp.*

Acknowledgments

The authors are grateful to Sylvain Enguehard (Novakits, Nantes) for providing the non-commercial primary antibodies necessary to carry out this study, as well as Nicolas Chomerat (from Ifremer, Concarneau) for sample transporting, and Adeline Bidault and Morgan Perennou (from LEMAR, Brest) for their support during sampling and dissections. We also thank Marie Calvez and Nelly Le Goïc (LEMAR, Brest) for their assistance with tissue

sectioning, and Carmen Rodríguez-Jaramillo (CIBNOR, La Paz) for her advices to optimize non-commercial antibodies for the IHC analysis. Thanks to Alejandra L. Peña for English edition.

Declaration of competing interest

The authors declare that they have no known competing financial interests or personal relationships that could have appeared to influence the work reported in this paper.

Funding

This work received financial support from the research project “MaSCoET” (Maintien du Stock de Coquillages en lien avec la problématique des Efflorescences Toxiques) financed by France Filière Pêche and Brest Métropole. JLGC is recipient of a doctorate fellowship from CONACyT, Mexico (REF: 2019- 000025-01EXTF-00067).

Data availability statement

The evidence and data that support the findings of this study are available from the corresponding author upon reasonable request.

Ethics statements

The organisms used in this work were transported and handled according to the International Standards for the Care and Use of Laboratory Animals. The number of sampled organisms contemplated "the rule of maximizing information published and minimizing unnecessary studies". In this sense, 38 individuals were considered the minimum number of organisms needed for this work.

Author contributions

Conceived the study: CF, HH, JLGC. Sampling: JLGC, HH, CF, ML, TD, AT. Processed the samples: JLGC, TD, AD, AT. Analyzed the data: JLGC, AD. Interpretation of data: JLGC, CF, HH, AD. Contributed reagents/materials/analysis tools: CF, HH, AD, AT, ML. Wrote the first draft of the manuscript: JLGC. Writing – review & editing: CF, HH, JLGC, ML, AD, AT.

Literature cited

Álvarez, G., Rengel, J., Araya, M., Álvarez, F., Pino, R., Uribe, E., Díaz, P.A., Rossignoli, A.E., López-Rivera, A., Blanco, J., 2020. Rapid domoic acid depuration in the scallop *Argopecten purpuratus* and its transfer from the digestive gland to other organs. *Toxins*, 12, 698. https://doi.org/10.3390/toxins12110698.

Amzil, Z., Fresnel, J., Le Gal, D., Billard, C., 2001. Domoic acid accumulation in French shellfish in relation to toxic species of *Pseudo-nitzschia multiseries* and *P. pseudodelicatissima*. *Toxicon*, 39(8), 1245–1251. https://doi.org/10.1016/s0041-0101(01)00096-4

Ayache, N., Hervé, F., Martin-Jézéquel, V., Amzil, Z., Caruana, A. M. N., 2018. Influence of sudden salinity variation on the physiology and domoic acid production by two strains of *Pseudo-nitzschia australis*. In T. Mock (Ed.), *Journal of Phycology*, 55(1), 186–195. https://doi.org/10.1111/jpy.12801.

Balbi, T., Cortese, K., Ciacci, C., Bellese, G., Vezzulli, L., Pruzzo, C., Canesi, L., 2018. Autophagic processes in *Mytilus galloprovincialis* hemocytes: effects of *Vibrio tapetis*. *Fish & Shellfish Immunology*. 73, 66–74. https://doi.org/10.1016/j.fsi.2017.12.003.

Baranska, A., Shawket, A., Jouve, M., Baratin, M., Malosse, C., Voluzan, O., Vu Manh, T.-P., Fiore, F., Bajénoff, M., Benaroch, P., Dalod, M., Malissen, M., Henri, S., Malissen, B., 2018. Unveiling skin macrophage dynamics explains both tattoo persistence and strenuous removal. *Journal of Experimental Medicine*, 215(4), 1115–1133. https://doi.org/10.1084/jem.20171608

Basti, L., Hégaret, H., Shumway, S.E., 2018. Harmful Algal Blooms and Shellfish. In: Harmful Algal Blooms: A Compendium Desk Reference, First Edition. Shumway, S.E., Burkholder, J.M., Morton, S.L. (eds). John Wiley & Sons Ltd.

Bates S.S., Garrison D.L., Horner R.A., 1998. Bloom dynamics and physiology of domoic-acid-producing *Pseudo-nitzschia* species. In: Physiological ecology of harmful algal multiseries.In: Harmful algal blooms 2000 (Ed. by G.M. Hallegraeff, S.I. Blackburn, C.J. Bolch & R.J. Lewis), pp. 320–323. Intergovernmental Oceanographic Commission of UNESCO, Paris.

Bates, S.S., Hubbard, K.A., Lundholm, N., Montresor, M., Leaw, C.P., 2018. *Pseudo-nitzschia, Nitzschia,* and domoic acid: new research since 2011. *Harmful Algae*, 79, 3-43. https://doi.org/10.1016/j.hal.2018.06.001.

618 Ben Haddouch, A., Taleb, H., Elmortaji, H., Ben Brahim, S., Ennafah, B., Menchih, K.,
619 Boumaz, A., Mzaki, F., Radi, A., Loutfi, M., 2016. Accumulation and tissue distribution of
620 domoic acid in the common cuttlefish, *Sepia officinalis* from the south Moroccan coast.
621 *American Academic Scientific Research Journal for Engineering, Technology, and*
622 *Sciences*, 15(1), 252–264.

623 Blanco, J., Acosta, C., Bermúdez de la Puente, M., Salgado, C., 2002a. Depuration and
624 anatomical distribution of the amnesic shellfish poisoning (ASP) toxin domoic acid in the
625 king scallop *Pecten maximus*. *Aquatic Toxicology*, 60 (1-2), 111–121.
626 https://doi.org/10.1016/s0166-445x(01)00274-0.

627 Blanco, J., Acosta, C.P., Mariño, C., Muñiz, S., Martín, H., Moroño, A., Correa, J., Arévalo,
628 F., Salgado, C., 2006. Depuration of domoic acid from different body compartments of the
629 king scallop *Pecten maximus* grown in raft culture and natural bed. *Aquatic Living*
630 *Resources*, 19 (3), 257–265. https://doi.org/10.1051/alr:2006026.

631 Blanco, J., Bermúdez, M., Arévalo, F., Salgado, C., Moroño, A., 2002b. Depuration of
632 mussels (*Mytilus galloprovincialis*) contaminated with domoic acid. *Aquatic Living*
633 *Resources*, 15, 53–60. https://doi.org/10.1016/S0990-7440(01)01139-1.

634 Blanco, J., Livramento, F., Rangel, I. M., 2010. Amnesic shellfish poisoning (ASP) toxins in
635 plankton and molluscs from Luanda Bay, Angola. *Toxicon*, 55(2–3), 541–546.
636 https://doi.org/10.1016/j.toxicon.2009.10.008.

637 Blanco, J., Moroño, A., Arévalo, F., Correa, J., Salgado, C., Rossignoli, A., Lamas, P., 2021.
638 Twenty-Five Years of Domoic Acid Monitoring in Galicia (NW Spain): Spatial, Temporal
639 and Interspecific Variations. *Toxins*, 13(11):756. https://doi.org/10.3390/toxins13110756.

640 Bogan, Y. M., Kennedy, D. J., Harkin, A. L., Gillespie, J., Vause, B. J., Beukers-Stewart, B.
641 D., Hess, P., Slater, J.W., 2007a. Variation in domoic acid concentration in king scallop
642 (*Pecten maximus*) from fishing grounds around the Isle of Man. *Harmful Algae*, 6, 81–92.
643 https://doi.org/10.1016/j.hal.2006.07.002.

644 Bogan, Y., Bender, K., Hervas, A., Kennedy, D., Slater, J., Hess, P., 2007c. Spatial variability
645 of domoic acid concentration in king scallops *Pecten maximus* off the southeast coast of
646 Ireland. *Harmful Algae*. 6(1): 1-14. https://doi.org/10.1016/j.hal.2006.05.004

Bogan, Y.M., Harkin, A.L., Gillespie, J., Kennedy, D.J., Hess, P., Slater, J.W., 2007b. The influence of size on domoic acid concentration in king scallop, *Pecten maximus* (L.). *Harmful Algae*, 6, 15–28. https://doi.org/10.1016/j.hal.2006.05.005.

Chi, C., Zhang, C., Liu, J., Zheng, X., 2019. Effects of marine toxin domoic acid on innate immune responses in bay scallop. Journal of Marine Science and Engineering, 7(11), 407. https://doi.org/10.3390/jmse7110407.

Costa, P. R., Rosa, R., Duarte-Silva, A., Brotas, V., Sampayo, M. A. M., 2005a. Accumulation, transformation and tissue distribution of domoic acid, the amnesic shellfish poisoning toxin, in the common cuttlefish, *Sepia officinalis*. *Aquatic Toxicology*, 74(1), 82–91. https://doi.org/10.1016/j.aquatox.2005.01.011

Costa, P. R., Rosa, R., Pereira, J., M. Sampayo., 2005b. Detection of domoic acid, the amnesic shellfish toxin, in the digestive gland of *Eledone cirrhosa* and *E. moschata* (Cephalopoda, Octopoda) from the Portuguese coast. *Aquatic Living Resources*, 18(4), 395–400). https://doi.org/10.1051/alr:2005041.

Costa, P. R., Rosa, R., Sampayo, M. A. M., 2004. Tissue distribution of the amnesic shellfish toxin, domoic acid, in *Octopus vulgaris* from the Portuguese coast. *Marine Biology*, 144(5), 971–976. https://doi.org/10.1007/s00227-003-1258-6.

Costa, P., Costa, M.H., 2012. Development and application of a novel histological multichrome technique for clam histopathology. *Journal of Invertebrate Pathology*, 110, 411–414. https://doi.org/10.1016/j.jip.2012.04.013.

Cuervo, A.M., 2004. Autophagy: many paths to the same end. *Molecular and Cellular Biochemistry*, 263 (1/2), 55–72. https://doi.org/10.1023/b:mcbi.0000041848.57020.57.

Dizer, H., Fischer, B., Harabawy, A.S.A., Hennion, M.C., Hansen, P.D., 2001. Toxicity of domoic acid in the marine mussel *Mytilus edulis*. *Aquatic Toxicology*, 55: 149-156. https://doi.org/10.1016/s0166-445x(01)00178-3.

Dusek Jennings, E., Parker, M. S., Simenstad, C. A., 2020. Domoic acid depuration by intertidal bivalves fed on toxin-producing *Pseudo-nitzschia multiseries*. *Toxicon*, 6, 100027. https://doi.org/10.1016/j.toxcx.2020.100027.

675 Flannagan, R. S., Jaumouillé, V., Grinstein, S., 2012. The Cell Biology of Phagocytosis.
676 *Annual Review of Pathology: Mechanisms of Disease*, 7(1), 61–98.
677 https://doi.org/10.1146/annurev-pathol-011811-132445.

678 García-Corona, J. L., Hégaret, H., Deléglise, M., Marzari, A., Rodríguez-Jaramillo, C.,
679 Foulon, V., Fabioux, C., 2022. First subcellular localization of the amnesic shellfish toxin,
680 domoic acid, in bivalve tissues: Deciphering the physiological mechanisms involved in its
681 long-retention in the king scallop *Pecten maximus*. *Harmful Algae*, 116.
682 https://doi.org/10.1016/j.hal.2022.102251.

683 Gilgan, M.W., Burns B.G., Landry, G.J., 1990. Distribution and magnitude of domoic acid
684 contamination of shellfish in Atlantic Canada. In: E. Graneli, B. Sundstrom, L. Edler, D.M.
685 Anderson (Eds.), Toxic Marine Phytoplankton. Elsevier, N.Y. pp. 469- 474.

686 Gómez-Robles, E., Rodríguez-Jaramillo, C., Saucedo, P.E., 2005. Digital image analysis of
687 lipid and protein histochemical markers for measuring oocyte development and quality in
688 pearl oyster *Pinctada mazatlanica* (Hanley, 1856). Journal of Shellfish Research, 24(4),
689 1197-1202. http://dx.doi.org/10.2983/0730-8000(2005)24[1197:DIAOLA]2.0.CO;2.

690 Gordon, S., 2016. Phagocytosis: An Immunobiologic Process. *Immunity*, 44(3), 463–475.
691 https://doi.org/10.1016/j.immuni.2016.02.026.

692 Haya, K., Martin, J.L., Burridge, L.E., Waiwood, B.A., Wildish, J., 1991. Domoic acid in
693 shellfish and plankton from the bay of Fundy, New Brunswick, Canada. *Journal of*
694 *Shellfish Research*, 10, 113–118.

695 Hector, A., 2015. The new statistics with R: an introduction for biologists, 1st ed. Oxford
696 University Press, New York.

697 Hégaret, H., Smolowitz, R. M., Sunila, I., Shumway, S. E., Alix, J., Dixon, M., Wikfors, G.
698 H., 2010. Combined effects of a parasite, QPX, and the harmful-alga, *Prorocentrum*
699 *minimum* on northern quahogs, *Mercenaria mercenaria*. *Marine Environmental Research*,
700 69(5), 337–344. https://doi.org/10.1016/j.marenvres.2009.12.008.

701 Horner, R.A., Kusske, M.B., Moynihan, B.P., Skinner, R.N., Wekell, J.C., 1993. Retention of
702 Domoic Acid by Pacific Razor Clams, *Siliqua patula* (Dixon, 1789): Preliminary Study.
703 *Journal of Shellfish Research*, 12, 451–456.

Husson, B., Hernández-Fariñas, T., Le Gendre, R., Schapira, M., Chapelle, A., 2016. Two decades of *Pseudo-nitzschia* spp. blooms and king scallop (*Pecten maximus*) contamination by domoic acid along the French Atlantic and English Channel coasts: Seasonal dynamics, spatial heterogeneity and interannual variability. *Harmful Algae*, 51, 26–39. https://doi.org/10.1016/j.hal.2015.10.017

James, K.D., Gillman, M., Fernández-Amandi, M., López- Rivera, A., Fernández Puente, P., Lehane, M., Mitrovic, S., Furey, A., 2005. Amnesic shellfish poisoning toxins in bivalve molluscs in Ireland. *Toxicon*, 46, 852–858. https://doi.org/10.1016/j.toxicon.2005.02.009.

Jones, T.O., Whyte, J.N.C., Ginther, N.G., Townsend, L.D., Iwama, G.K., 1995. Haemocyte changes in the pacific oyster, *Crassostrea gigas*, caused by exposure to domoic acid in the diatom *Pseudo-nitzschia pungens* f. *multiseries*. *Toxicon*, 33 (3), 347–353. https://doi.org/10.1016/0041-0101(94)00170-.

Kim, Y., Ashton-Alcox, K.A., Powell, E.N., 2006. Histological Techniques for Marine Bivalve Molluscs: update. NOAA Technical Memorandum NOS NCCOS 27, Maryland.

Klionsky, D. J., Eskelinen, E.-L., Deretic, V., 2014. Autophagosomes, phagosomes, autolysosomes, phagolysosomes, autophagolysosomes… Wait, I'm confused. *Autophagy*, 10 (4), 549–551. https://doi.org/10.4161/auto.28448.

Kvrgić, K., Lešić, T., Džafić, N., Pleadin, P., 2022. Occurrence and seasonal monitoring of domoic acid in three shellfish species from the Northern Adriatic Sea. *Toxins*, 14(1), 33; https://doi.org/10.3390/toxins14010033.

La Barre, S., Bates, S.S. Quilliam, M.A., 2014. Domoic acid. In. Outstanding marine molecules: chemistry, biology, analysis. Edited by S. La Barre and J.-M. Kornprobst. Wiley-VCH Verlag GmbH & Co. KgaA, Weinheim, Germany, pp. 189–216.

Lassudrie, M., Soudant, P., Richard, G., Henry, N., Medhioub, W., da Silva, P. M., Donval, A., Bunel, M., Le Goïc, N., Lambert, C., de Montaudouin, X., Fabioux, C., Hégaret, H., 2014. Physiological responses of Manila clams *Venerupis* (=*Ruditapes*) *philippinarum* with varying parasite *Perkinsus olseni* burden to toxic algal *Alexandrium ostenfeldii* exposure. *Aquatic Toxicology*, 154, 27–38. https://doi.org/10.1016/j.aquatox.2014.05.002.

Lelong, A., Hégaret, H., Soudant, P., Bates, S.S., 2012. *Pseudo-nitzschia* (Bacillariophyceae) species, domoic acid and amnesic shellfish poisoning: revisiting previous paradigms. *Phycologia*, 51 (2), 168–216. https://doi.org/10.2216/11-37.1.

735 Liu, H., Kelly, M.S., Campbell, D.A., Dong, S.L., Zhu, J.X., Fang, J.G., Wang, S.F., 2007a.
736 Exposure to domoic acid affects larval development of king scallop *Pecten maximus*
737 (Linnaeus, 1758). *Aquatic Toxicology*, 81, 152–158.
738 https://doi.org/10.1016/j.aquatox.2006.11.012.

739 Liu, H., Kelly, M.S., Campbell, D.A., Dong, S.L., Zhu, J.X., Wang, S.F., 2007b. Ingestion of
740 domoic acid and its impact on king scallop *Pecten maximus* (Linnaeus, 1758). *Journal of*
741 *Ocean University of China*, 6, 175–181. https://doi.org/10.1007/s11802-007-0175-6.

742 Mafra, L.L., Bricelj, V.M., Fennel, K., 2010. Domoic acid uptake and elimination kinetics in
743 oysters and mussels in relation to body size and anatomical distribution of toxin. *Aquatic*
744 *Toxicology*, 100 (1), 17–29. https://doi.org/10.1016/j.aquatox.2010.07.0.

745 Mauríz, A., Blanco, J., 2010. Distribution and linkage of domoic acid (amnesic shellfish
746 poisoning toxins) in subcellular fractions of the digestive gland of the scallop *Pecten*
747 *maximus*. *Toxicon*, 55 (2-3), 606–611. https://doi.org/10.1016/j.toxicon.2009.10.

748 McMillan, D.B., Harris, R.J., 2018. The Animal Cell. In An Atlas of Comparative Vertebrate
749 Histology (pp. 3–25). Elsevier. https://doi.org/10.1016/b978-0-12-410424-2.00001-9.

750 Moore, M.N., 2004. Diet restriction induced autophagy: a lysosomal protective system against
751 oxidative- and pollutant-stress and cell injury. *Marine Environmental Research*, 58 (2–5),
752 603–607. https://doi.org/10.1016/j.marenvres.2004.03.

753 Moore, M.N., 2008. Autophagy as a second level protective process in conferring resistance
754 to environmentally-induced oxidative stress. *Autophagy*, 4 (2), 254–256.
755 https://doi.org/10.4161/auto.5528.

756 Novaczek, I., Madhyastha, M.S., Ablett, R.F., Donald, A., Johnson, G., Nijjar, M.S., Sims,
757 D.E., 1992. Depuration of domoic acid from live blue mussels (*Mytilus edulis*). *Canadian*
758 *Journal of Fisheries and Aquatic Sciences*, 49 (2), 312–318. https://doi.org/10.1139/f92-
759 035.

760 O'Dea, S.N., 2012. Occurrence, Toxicity, and Diversity of *Pseudo-nitzschia* in Florida
761 Coastal Waters. University of South Florida ProQuest Dissertations Publishing. 1515837.

762 Pazos, A.J., Ventoso, P., Martínez-Escauriaza, R., Pérez-Parallé, M.L., Blanco, J., Triviño,
763 J.C., Sánchez, J.L., 2017. Transcriptional response after exposure to domoic acid-

764 producing *Pseudo-nitzschia* in the digestive gland of the mussel *Mytilus galloprovincialis*.
765 *Toxicon*, 140, 60–71. https://doi.org/10.1016/j.toxicon.2017.10.002.

766 Perl, T.M., Bédard, L., Kosatsky, T., Hockin, J.C., Todd, E.C.D., Remis, R.S., 1990. An
767 Outbreak of Toxic Encephalopathy Caused by Eating Mussels Contaminated with Domoic
768 Acid. *N. Engl. J. Med.* 322(25): 1775–1780. https://doi:10.1056/NEJM199006213222504.

769 Picot, S., Morga, B., Faury, N., Chollet, B., Dégremont, L., Travers, M.A., Renault, T., Arzul,
770 I., 2019. A study of autophagy in hemocytes of the Pacific oyster *Crassostrea gigas*.
771 *Autophagy*, 1–9. https://doi.org/10.1080/15548627.2019.1596.

772 Pulido, O.M., 2008. Domoic Acid Toxicologic Pathology: A Review. *Marine Drugs*, 6, 180-
773 219. https://doi.org/10.3390/md20080010.

774 Quilliam, M.A., Sim, P.G., McCulloch, A.W., McInnes, A.G., 1989. High-performance liquid
775 chromatography of domoic acid, a marine neurotoxin, with application to shellfish and
776 plankton. *International Journal of Environmental Analytical Chemistry*, 36 (3), 139–154.
777 https://doi.org/10.1080/03067318908026867.

778 R Core Team (2020). R: a language and environment for statistical computing. R Foundation
779 for Statistical Computing, Vienna, Austria. URL https://www.R-project.org/.

780 Rodríguez-Jaramillo, C., García-Corona, J.L., Zenteno-Savín, T., Palacios, E., 2022. The
781 effects of experimental temperature increase on gametogenesis and heat stress parameters
782 in oysters: Comparison of a temperate-introduced species (*Crassostrea gigas*) and a native
783 tropical species (*Crassostrea corteziensis*). *Aquaculture*, 561, 738683.
784 https://doi.org/10.1016/j.aquaculture.2022.738683.

785 Shubin, A. V., Demidyuk, I. V., Komissarov, A. A., Rafieva, L. M., & Kostrov, S. V., 2016.
786 Cytoplasmic vacuolization in cell death and survival. *Oncotarget*, 7(34), 55863–55889.
787 https://doi.org/10.18632/oncotarget.10150.

788 Silvert, W. and Subba R.D.V., 1992. Dynamic model of the flux of domoic acid, a neurotoxin,
789 through a *Mytilus edulis* population. *Canadian Journal of Fisheries and Aquatic Sciences*,
790 49, 400- 405. https://doi.org/10.1139/f92-045.

791 Takata, Y., Sato, S., Ha, D. V., Montojo, U. M., Lirdwitayaprasit, T., Kamolsiripichaiporn, S.,
792 Kotaki, Y., Fukuyo, Y., Kodama, M., 2009. Occurrence of domoic acid in tropical
793 bivalves. *Fisheries Science*, 75(2), 473–480. https://doi.org/10.1007/s12562-009-0073-5.

794 Trainer, V.L., Bates, S.S., Lundholm, N., Thessen, A.E., Cochlan, W.P., Adams, N.G., 2012.
795 *Pseudo-nitzschia* physiological ecology, phylogeny, toxicity, monitoring and impacts on
796 ecosystem health. *Harmful Algae*, 14, 271–300. https://doi.org/10.1016/j.hal.2011.10.025.

797 Trainer, V.L., Bill, B.D., 2004. Characterization of a domoic acid binding site from Pacific
798 razor clam. *Aquatic Toxicology*, 69, 125–132.
799 https://doi.org/10.1016/j.aquatox.2004.04.012.

800 Vale, P., Sampayo, M.A.M., 2001. Domoic acid in Portuguese shellfish and fish. *Toxicon*,
801 39:893–904. https://doi.org/10.1016/s0041-0101(00)00229-4.

802 Ventoso, P., Pazos, A.J., Blanco, J., Pérez-Parallé, M.L., Triviño, J.C., Sánchez, J.L., 2021.
803 Transcriptional Response in the Digestive Gland of the King Scallop (*Pecten maximus*)
804 After the Injection of Domoic Acid. *Toxins*, 13, 339.
805 https://doi.org/10.3390/toxins13050339.

806 Ventoso, P., Pazos, A.J., Pérez-Parallé, M.L., Blanco, J., Triviño, J.C., Sánchez, J.L., 2019.
807 RNA-Seq Transcriptome Profiling of the Queen Scallop (*Aequipecten Opercularis*)
808 Digestive Gland after Exposure to Domoic Acid-Producing *Pseudo-nitzschia*. *Toxins*, 11,
809 97. https://doi.org/10.3390/toxins11020097.

810 Wang, L., Ye, X., Zhao, T., 2019. The physiological roles of autophagy in the mammalian life
811 cycle. *Biological Reviews*, 94, 503–516. https://doi.org/10.1111/brv.12464.

812 Wright, J.L., Bird, C.J., de Freitas, A.S., Hampson, D., McDonald, J., Quilliam, M.A., 1990a.
813 Chemistry, biology, and toxicology of domoic acid and its isomers. Canada Diseases
814 Weekly Report = Rapport Hebdomadaire des Maladies au Canada. Pp. 21-26.

815 Wright, J.L.C., Falk, M., McInnes, A.G., Walter, J.A., 1990b. Identification of isodomoic acid
816 D and two new geometrical isomers of domoic acid in toxic mussels. *Canadian Journal of*
817 *Chemistry*, 68(1), 22–25. https://doi.org/10.1139/v90-005.

818 Zar, J. H., 2010. Biostatistical Analysis. 5th Ed. Pearson, Westlake Village, CA, 251 pp.

819 Zhao, Y.G., Codogno, P., Zhang, H., 2021. Machinery, regulation and pathophysiological
820 implications of autophagosome maturation. *Nature Reviews Molecular Cell Biology*.
821 https://doi.org/10.1038/s41580-021-00392-4.

822 Zheng, G., Wu, H., Guo, M., Peng, J., Zhai, Y., Tan, Z., 2022. First observation of domoic
823 acid and its isomers in shellfish samples from Shandong Province, China. *Journal of*

Oceanology and Limnology, 40(6), 2231–2241. https://doi.org/10.1007/s00343-022-2104-3.

Table 1. Relative abundance of DA and its isomers in the digestive glands of the scallops *P. maximus* (n =5) and *A. opercularis* (n =10), the clam *D. trunculus* (n =11), the slippersnail *C. fornicata* (n =7), and the sea squirt *Asterocarpa* sp. (n =5) contaminated during *P. australis* blooms in the northwest coast of Brittany, France between March-April 2021.

	Species					Statistical analysis	
	P. maximus	*A. opercularis*	*D. trunculus*	*C. fornicata*	*Asterocarpa sp.*		
DA (%)	93.3 ± 0.6^{b}	93.6 ± 0.3^{b}	95.8 ± 0.3^{a}	90.7 ± 1.1^{c}	94.5 ± 0.1^{ab}	$F_{(df=4,33)} = 11.8,$	$P < 0.0001$
isoE (%)	4.3 ± 0.3^{a}	4.3 ± 0.3^{a}	3.5 ± 0.3^{a}	3.2 ± 0.4^{a}	1.6 ± 0.1^{b}	$F_{(df=4,33)} = 10.9,$	$P < 0.0001$
isoD (%)	1.5 ± 0.3^{bc}	1 ± 0.1^{bc}	0.5 ± 0.1^{c}	4 ± 0.8^{a}	2.1 ± 0.0^{b}	$F_{(df=4,33)} = 17.3,$	$P < 0.0001$
isoA (%)	0.4 ± 0.0^{ab}	0.7 ± 0.0^{a}	0.2 ± 0.0^{b}	0.6 ± 0.1^{a}	0.5 ± 0.0^{a}	$F_{(df=4,33)} = 10.4,$	$P < 0.0001$
epi-DA (%)	0.4 ± 0.1^{b}	$0.4 \pm 0°0^{b}$	0 ± 0.0^{c}	1.5 ± 0.1^{a}	1.3 ± 0.0^{a}	$F_{(df=4,33)} = 156.4,$	$P < 0.0001$

Results are expressed as mean ± SE. Data were analyzed using species (five levels) as factor in separate one-way ANOVAs ($P < 0.05$). The F-test statistic and degrees of freedom (df) are reported. Different superscript letters indicate significant differences between species. The level of statistical significance was set at $\alpha = 0.05$.

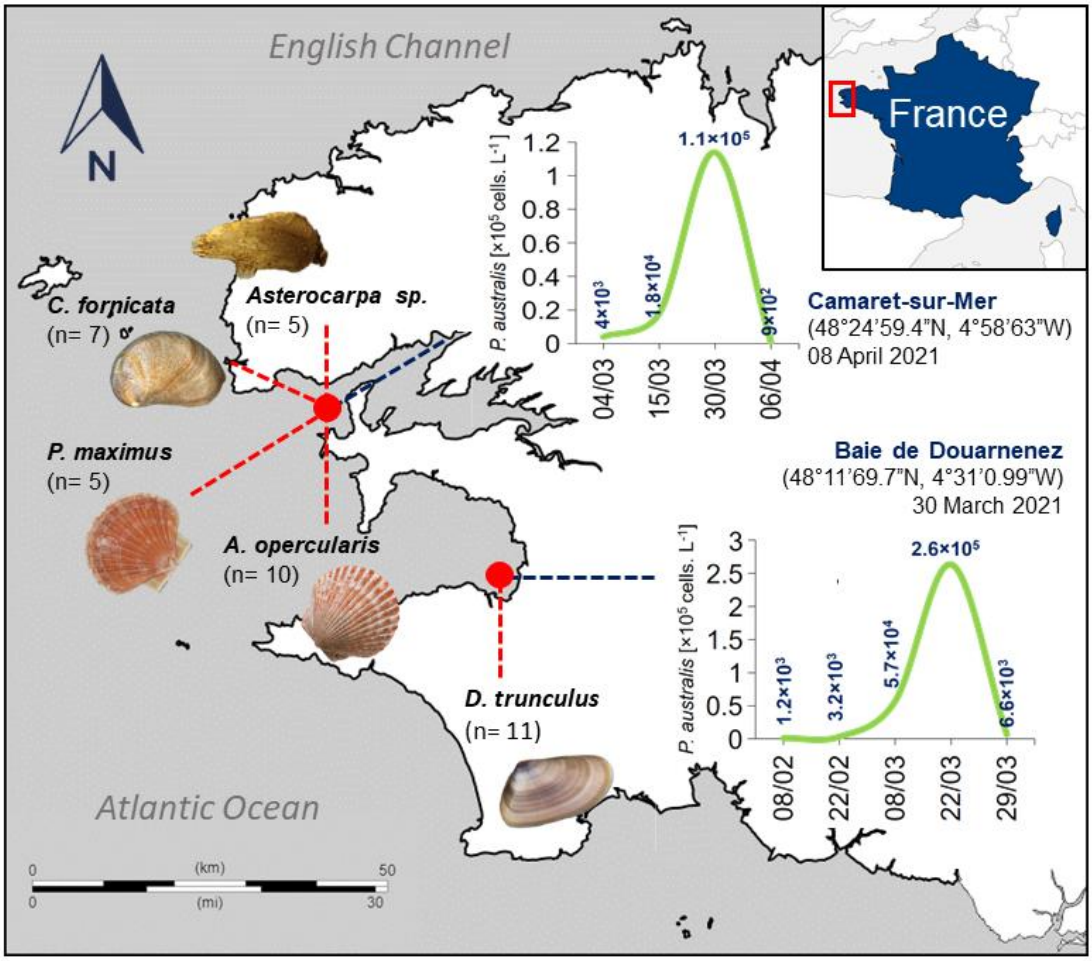

832

833 **Figure 1.** Sampling sites of the scallops *P. maximus* (n =5) and *A. opercularis* (n = 10), the
834 clam *D. trunculus* (n =11), the slippersnail *C. fornicata* (n =7), and the sea squirt *Asterocarpa*
835 *sp.* (n =5) and cell densities (cells. L^{-1}) of *P. australis* during toxic blooms in the northwest
836 coast of Brittany, France between February and-April 2021.

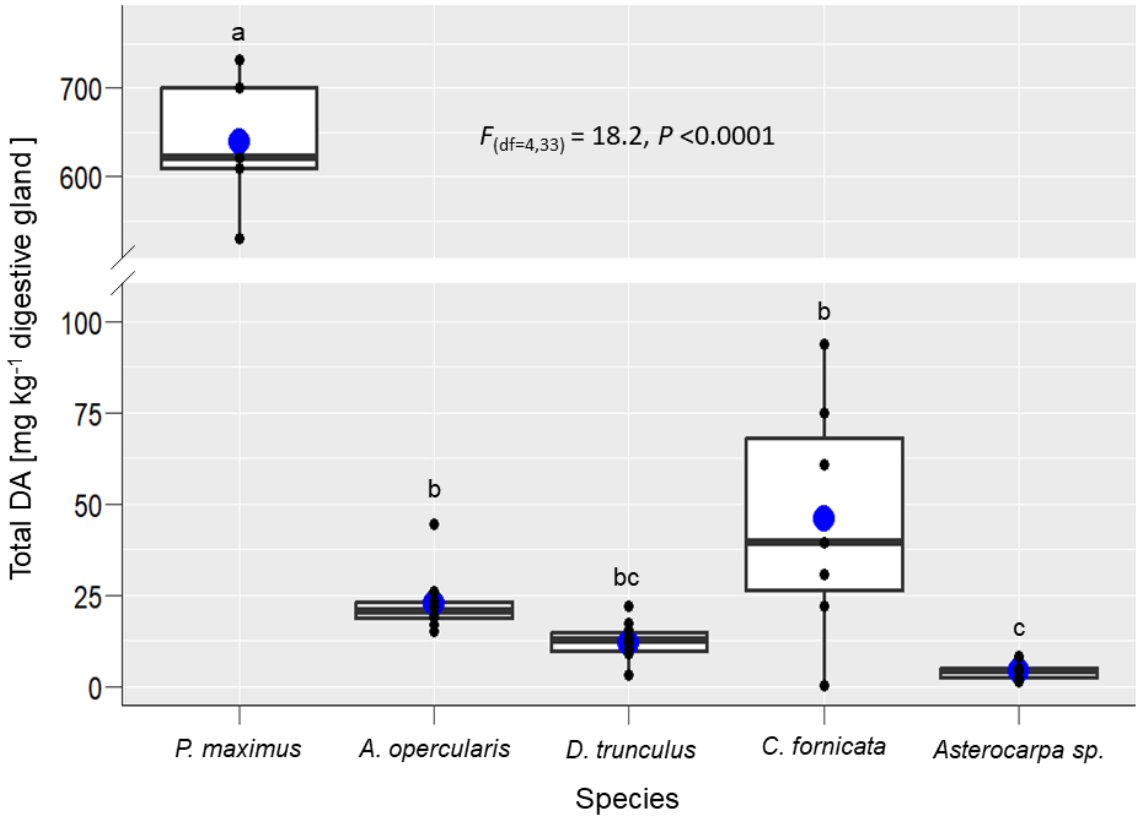

Figure 2. Total domoic acid (tDA) concentration in the digestive glands of the scallops *P. maximus* (n =5) and *A. opercularis* (n = 10), the clam *D. trunculus* (n =11), the slippersnail *C. fornicata* (n =7), and the sea squirt *Asterocarpa sp.* (n =5) contaminated during *P. australis* blooms in the northwest coast of Brittany, France between on the 30th of March (for the scallops *P. maximus*, *A. opercularis*, the slippersnail *C. fornicata*, and the sea squirt *Asterocarpa sp.*) and on the 8th of April, 2021 (for the clam *D. trunculus*). The upper and lower limits of the boxes are the quartiles, the middle horizontal line is the median, the extremes of the vertical lines are the upper and lower limits of the observations, and black dots are the individual observations. The blue dots are the means for each species. Data were analyzed using species (five levels) as factor using a one-way ANOVA (P <0.05). The F-test statistic and degrees of freedom (df) are reported. Different superscript letters indicate significant differences between species. The level of statistical significance was set at α =0.05.

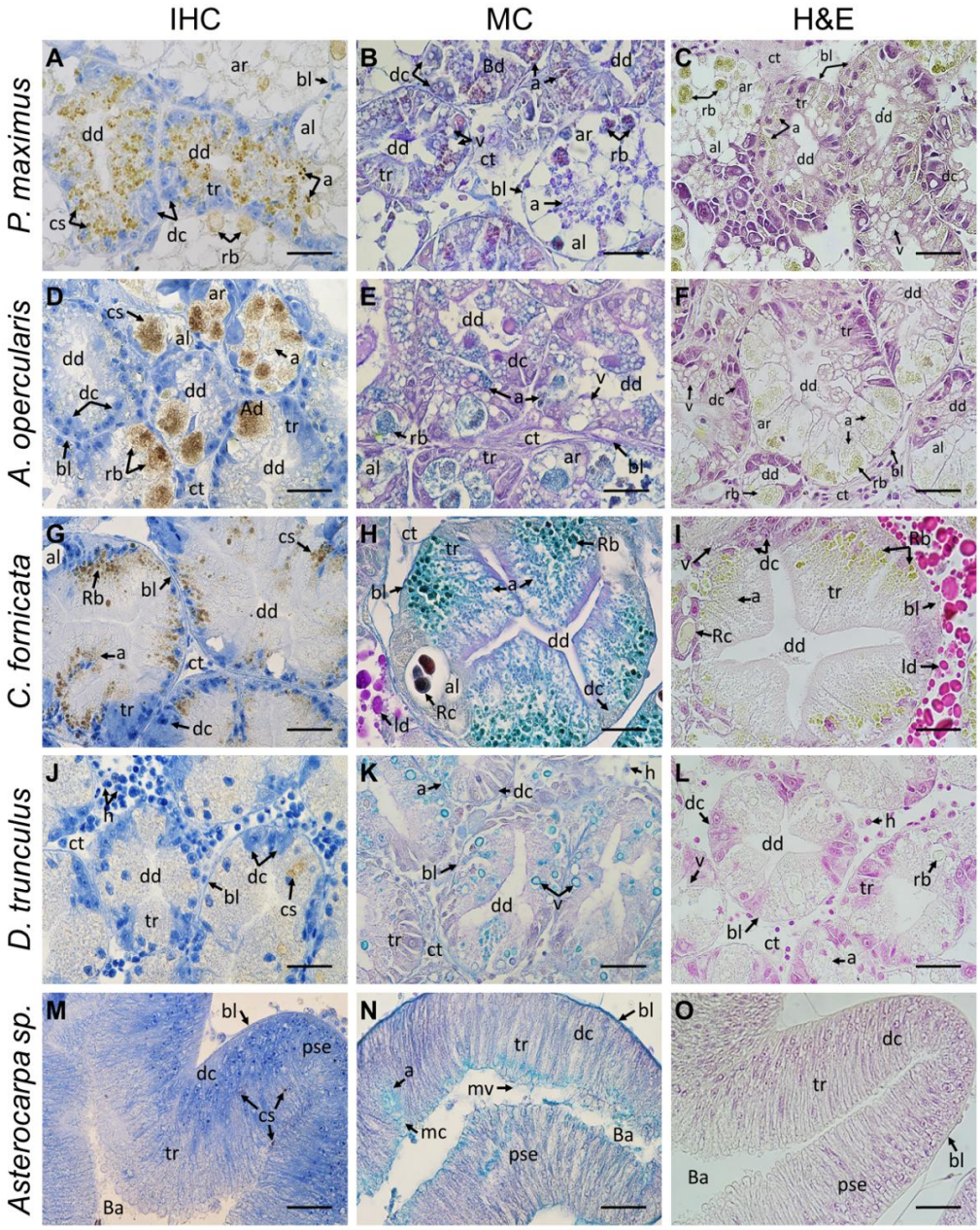

851

852 **Figure 3.** Microphotographs of digestive glands of the scallops *P. maximus* (A, B, C), *A.*
853 *opercularis* (D, E, F), the slippersnail *C. fornicata* (G, H, I), the clam *D. trunculus* (J, K, L),
854 and the sea squirt *Asterocarpa* sp. (M, N, O) contaminated with domoic acid (DA) during *P.*
855 *australis* blooms in the northwest coast of Brittany, France in March-April, 2021. IHC (A, D,
856 G, J, M) = Immunohistochemical detection of DA using specific anti-DA antibody (0.08 mg.
857 mL^{-1}); MC (B, E, H, K, N) = multichromic histochemical staining of neutral carbohydrates
858 (violet-magenta dyes), acid glycoconjugates (blue hues), and proteins (yellowish tones); H&E
859 (C, F, I, L, O) = conventional histological Hematoxylin-Eosin staining. a = autophagosomic-
860 like vesicles, al = adipocyte-like cell, ar = acinar region, Ba = blind ampulla, bl = basal
861 lamina, cs = DA chromogenic signal, ct = connective tissue, dc = digestive cells, dd =
862 digestive diverticulum, hc = hemocytes, ld = lipid droplets, mc = mucus, mv = microvilli, pse
863 = pseudostratified epithelium, rb = residual bodies, rc = residual concretions, tr = tubular
864 region, v = vacuoles. Scale bar: 63 × = 30 µm.

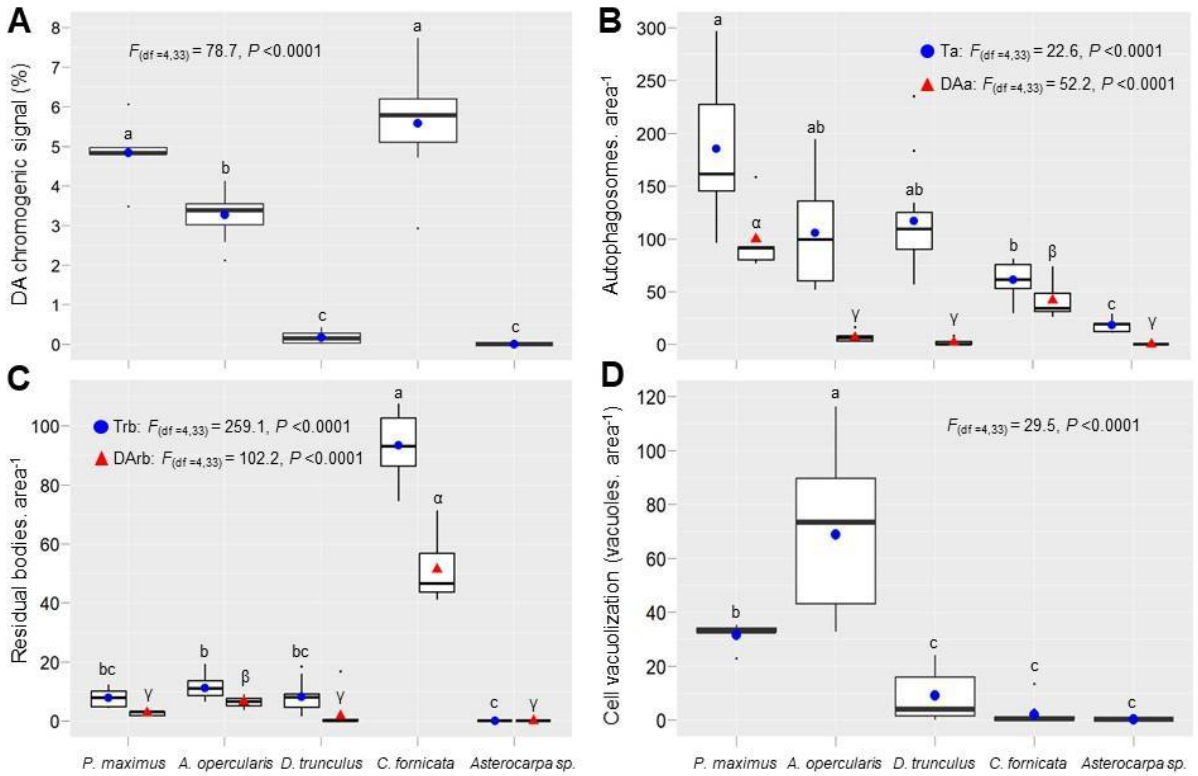

Figure 4. Quantitative analysis of DA localization and subcellular features in the digestive glands of the scallops *P. maximus* (n =5) and *A. opercularis* (n =10), the clam *D. trunculus* (n =11), the slippersnail *C. fornicata* (n =7) and the sea squirt *Asterocarpa* sp. (n =5) contaminated with DA during *P. australis* blooms in the northwest coast of Brittany, France, in March-April, 2021. (A) DA chromogenic signal (%); (B) Autophagy (autophagosomes. 1.3 mm^2, Ta = total autophagy, DAa = DA autophagy); (C) Residual bodies (residual bodies. 1.3 mm^2, Trb = total residual bodies, DArb = DA in the residual bodies); (D) Cell vacuolization (vacuoles. 1.3 mm^2). The upper and lower limits of the boxes are the quartiles, the middle horizontal line is the median, the extremes of the vertical lines are the upper and lower limits of the observations, and black dots are the outliers (values that deviate from the median more than 1.5 times the interquartile range). The blue dots and red triangles are the means of each variable. Data were analyzed using species (five levels) as factor in separate one-way ANOVA's (P <0.05). The F-test statistic and degrees of freedom (df) are reported. Different superscript letters indicate significant differences between species. The level of statistical significance was set at α =0.05.

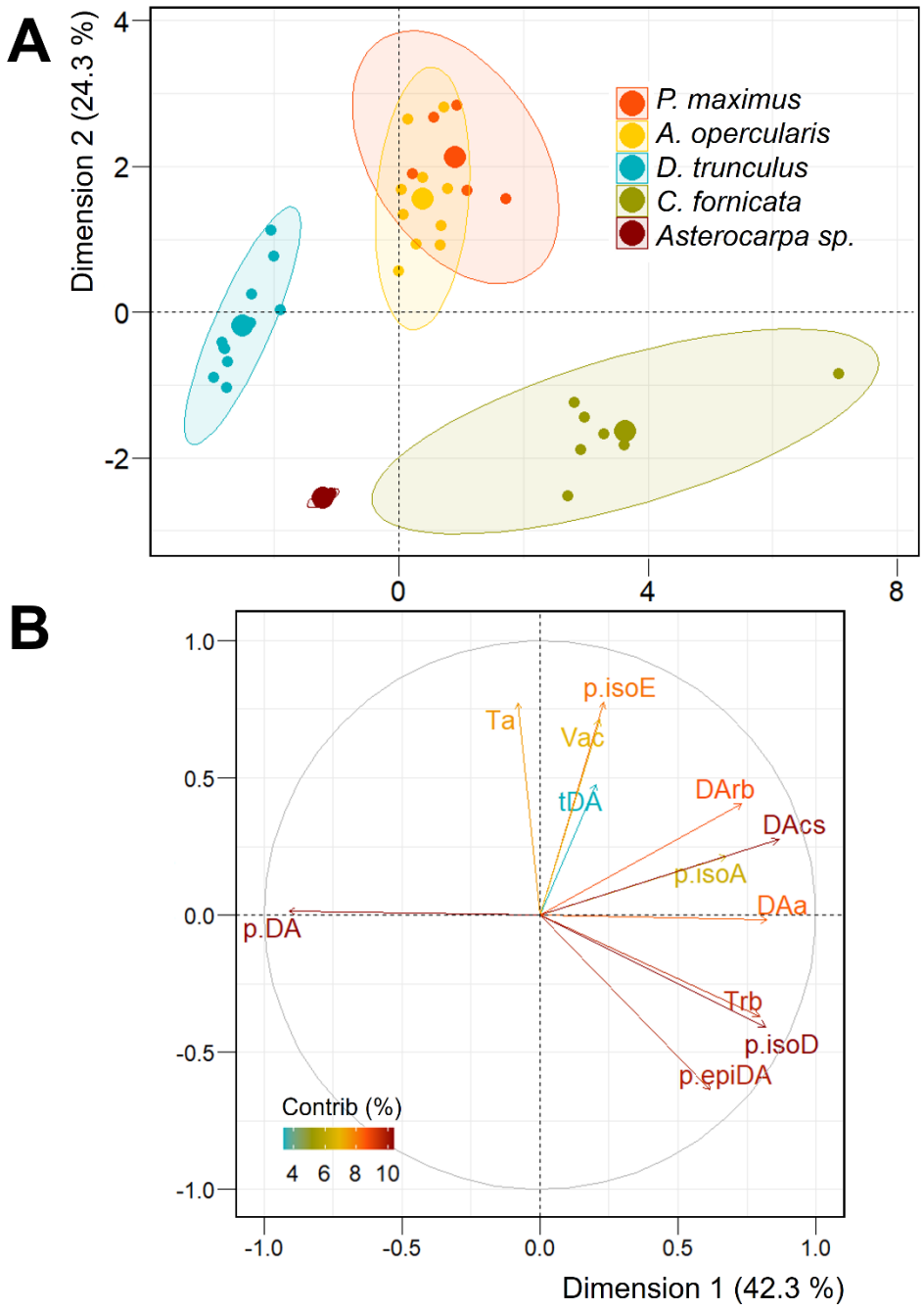

881

882 **Figure 5.** Principal component analysis (PCA) summarizing data from the scallops *P.*
883 *maximus* (n =5) and *A. opercularis* (n =10), the clam *D. trunculus* (n =11), the slippersnail *C.*
884 *fornicata* (n =7), and the sea squirt *Asterocarpa* sp. (n =5) contaminated with domoic acid
885 (DA) during *P. australis* blooms in the northwest coast of Brittany, France, between March-
886 April 2021. Dimension 1 and dimension 2 together describe 66.6 % of the total variance. (A)
887 Scatter plot of individuals from each species. Larger symbols are the barycenter of each
888 group, confidence ellipses level was fixed at α =0.05. (B) Variable contribution plot. The
889 direction of the arrows shows the correlations of variables (tDA = total DA, DAcs = DA
890 chromogenic signal, Ta = total autophagy, DAa = DA autophagy (%), Trb = total residual
891 bodies, DArb = DA in the residual bodies (%), Vac = cell vacuolization, and the percentages
892 (p) of DA isomers, p.DA = untransformed DA, p.isoE = isoE, p.isoD = isoD, p.isoA = isoA,

p.epiDA = epiDA) with given PCs, and its color intensity shows their contribution (Contrib %) to the explained variance.